Electrochemistry Communications 111 (2020) 106662

Contents lists available at ScienceDirect

Electrochemistry Communications

journal homepage: www.elsevier.com/locate/elecom

Electrospun conductive gold covered polycaprolactone fibers as electrochemical sensors for O_2 monitoring in cell culture media

Ariana Serban, Alexandru Evanghelidis, Melania Onea, Victor Diculescu, Ionut Enculescu, Madalina M. Barsan*

National Institute of Materials Physics, Atomistilor Str. 405A, 077125 Magurele, Romania

ARTICLE INFO

Keywords:
Electrospun fibers
Polycaprolactone
Oxygen sensor
Cellular media

ABSTRACT

This work reports the use of electrospun conductive gold covered polycaprolactone fibers for the quantification of dissolved O_2. The morphologies of the electrospun fibers obtained at a static and a dynamic drum collector were investigated by scanning electron microscopy. The reduction process of O_2 at negative potentials is analyzed by cyclic voltammetry and electrochemical impedance spectroscopy (EIS) in sodium phosphate buffer (NaPB) pH 7.0 and in cellular media pH 7.4. The electrochemical sensing performance of Au/PCL towards O_2 quantification in NaPB and cellular media is compared by using three electrochemical techniques: cyclic and linear sweep voltammetry and EIS. Measurements are done in a two electrode configuration, using a silver wire as reference, to show the applicability of the method for O_2 quantification in cellular culture media.

1. Introduction

Electrospun nanoscale polymeric fibers have been the focus of many research lines in the sensor development area, since their morphology and structure can be controlled during the fabrication process which lead to materials with large surface areas and high porosity, bringing innumerous advantages when immobilized on top of solid electrodes [1]. Flexible meshes of submicronic diameter polymer fibers fabricated by electrospinning found a variety of applications [2]. More recently, their coverage with metal [3] and metal/conducting polymer [4,5] turned them into electroactive self-standing devices, being recently used as flexible hydrogel embedded pH-sensors that can be integrated in inexpensive wearable and non-invasive devices [3].

Frameworks made up of electrospun polymeric fibers have also gained interest and applicability in the medical area, due to the slow biodegradation and biocompatible characteristics [6] with very promising applicability in tissue engineering [7–9]. Among them, electrospun polycaprolactone (PCL) fibers [9–11] have many medical applications since they are able to mimic the natural extra cellular morphology (ECM) and thus promote optimal cell growth. However, their structure [11] and solvent evaporation after electrospinning are crucial for their application in medical area [12,13].

Monitoring O_2 levels in 3D tissue constructs is crucial for many tissue engineering applications since the delivery of sufficient O_2 supply is the key for the survival of cells within the scaffold [14]. Due to tissue thickness and diffusion barriers many cells are prone to apoptosis after tissue implant [15]. We propose a fiber mesh made of electrospun PCL fibers covered with Au as a self-standing sensing platform for O_2 detection via electrochemical methods. The PCL scaffold will enable cells to grow, with the Au layer ensuring its electrochemical functionality. PCL fibers were electrospun following two procedures – static and dynamic – and covered with Au by magnetron sputtering, their morphology and structure being first analyzed by scanning electron microscopy (SEM). Dissolved O_2 levels were measured in phosphate buffer and cellular media by cyclic voltammetry (CV), linear sweep voltammetry (LSV) and electrochemical impedance spectroscopy (EIS). The obtained results are very promising for in vivo O_2 monitoring in cell culture.

2. Experimental section

2.1. Reagents and solutions

Polycaprolactone, chloroform, dimethylformamide (DMF), Na_2SO_3, NaH_2PO_4, Na_2HPO_4 were obtained from Sigma-Aldrich. Polyethylene terephthalate (PET) (0.038 mm) foils were from Good Fellow. Cell culture media was DMEM – Dulbecco's Modified Eagle Medium, from Thermo Fisher Scientific, and contained amino acids, inorganic salts, vitamins and glucose. Buffer electrolyte solutions of sodium phosphate (NaH_2PO_4 + Na_2HPO_4) 0.1 M pH 7.0, (NaPB) were prepared using

* Corresponding author.
E-mail address: madalina.barsan@infim.ro (M.M. Barsan).

https://doi.org/10.1016/j.elecom.2020.106662
Received 4 December 2019; Received in revised form 20 December 2019; Accepted 6 January 2020
Available online 24 January 2020

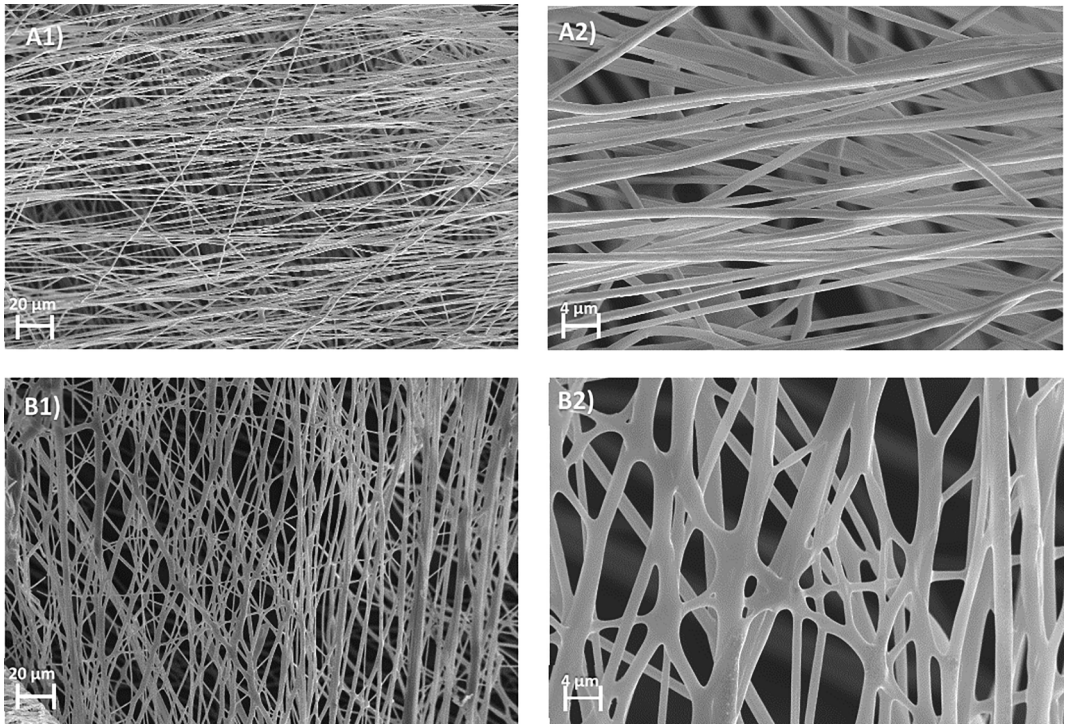

Fig. 1. SEM images at Au coated PCL electrospun fibers collected on A) a static and B) rotating collector.

analytical grade reagents and deionized water from a Millipore Milli-Q system (conductivity ≤ 0.1 µS cm^{-1}). Aliquots of 0.1 M Na_2SO_3 stock solution were added to get 0.2 mM sulfite in the cell, which corresponds to the consumption of 1 mM dissolved O_2, following the equation $Na_2SO_3 + ½\ O_2 \rightarrow Na_2SO_4$. The pH measurements were done with a Hannah pH-meter. All experiments were carried out at room temperature (25 ± 1 °C).

2.2. Fabrication of the O_2 sensor

Sensor fabrication involved two steps. First, polymer fibers were obtained by electrospinning a 16% PCL solution in 4:1 w/V chloroform:DMF, at 1.5 mL/h under 15 kV applied potential on the spinneret; the fibers were collected for 30 min on copper frames placed at 15 cm away from the spinneret. In the case of the rotating collector system, the copper frames were attached to a DC electric motor and grounded by connecting them with a thin, flexible copper wire to a larger plate collector situated 8 cm behind. Secondly, PCL fiber mats were covered with Au by magnetron sputtering with a 200 nm metallic layer (Au/PCL). The Au film thickness was determined previously by SEM imaging of angled and broken fibers corroborated with profilometry on flat Si/SiO_2 wafers covered with a Au layer using the same procedure. The thickness was chosen from previous methodologies perfected for covering other polymer based electrospun fibers, and it was thin enough to ensure full coverage of the fiber but not too thick, since it was also observed that thicker Au films lead to easily breakable fibers, with the Au layer tending to exfoliate [16].

Au/PCL fibers were thermally attached onto flexible thermoadhesive PET substrates by heating the ensemble at 150 °C, after the removal of the copper frame.

2.3. Methods

Structural and morphological characterization was carried out by scanning electron microscopy (SEM) at a Zeiss Evo 50 XVP. The SEM images were acquired at the magnifications of 5 and 50 kV, at 15 mm, with an accelerating voltage of 20 kV and a spot size of 300.

Electrochemical measurements were performed using an Ivium Compactstat.h. EIS parameters were: rms perturbation of 10 mV, frequency range 65 kHz-1 Hz, 10 frequency values per decade. The applied potential was −0.4 V, chosen close to the O_2 reduction peak from CV experiments. Data were analyzed using a ZView software, Scribner Associates USA.

The electrochemical cell had a two electrode configuration with the Au/PCL as working electrode and a Ag wire as counter and reference electrodes.

3. Results and discussion

3.1. Scanning electron microscopy

Fig. 1 displays SEM images of PCL electrospun fibers collected on A) a static and B) a dynamic collector, for 30 min, presenting a typical morphology for a polymer electrospun fiber. On the static collector fibers had similar diameters, of ≈1 µm and were aligned preferentially on one direction in the same plane. The dynamic collector distributed the fibers randomly with no preferential alignments and numerous ramifications. The fibers in Fig. 1B had diameters of different sizes of 1–4 µm. The fibers obtained using the static collector presented inferior mechanical strength and broke easily when manipulated for the electrochemical measurements. Therefore, fibers obtained at the dynamic drum collector where used in subsequent experiments.

3.2. Electrochemical characterization of Au/PCL electrodes

3.2.1. Cyclic voltammetry

CVs of a conventional Au bulk and Au/PCL electrode were recorded at 100 mV s^{-1} in a O_2 saturated NaPB solution, with similar profiles and with significantly higher currents recorded at Au/PCL due to its higher surface area (Fig. 2A). The electroactive area of the Au/PCL electrode was estimated to be at least 2.5 fold higher than the geometric area, from the cyclic voltammetry study performed at different scan rates in a solution containing the standard electroactive species $K_4[Fe(CN)_6]$ (data not shown). The CVs presented two oxidation peaks at 0.3

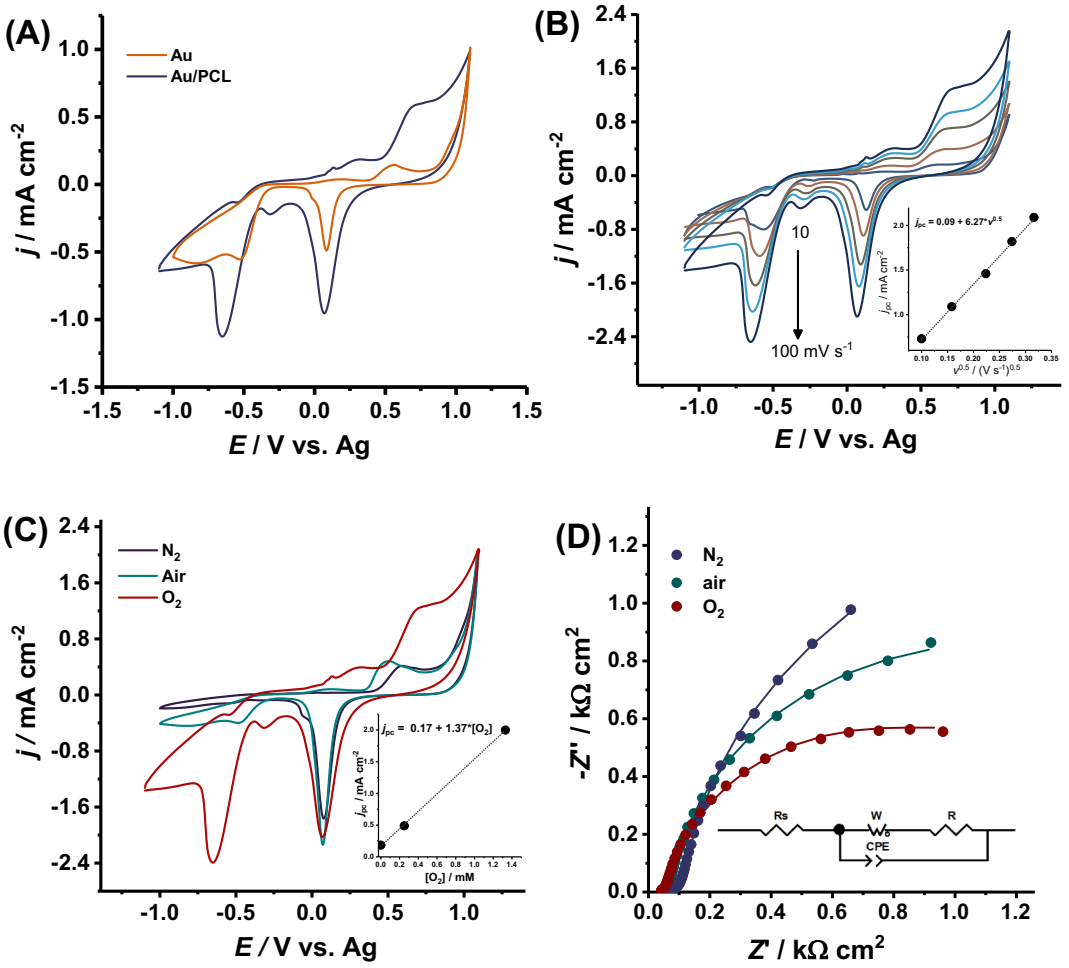

Fig. 2. A,B: CVs recorded in O_2 saturated 0.1 M NaPB solutions at A) a conventional Au bulk electrode and Au/PCl (50 mV s^{-1}) and B) Au/PCL at different scan rates (inset is the linear dependency of j_{pc} vs. $v^{0.5}$); C) CVs (100 mV s^{-1}; inset j_{pc} vs. $[O_2]$) and D) Complex plane impedance plots (-0.4 V) at Au/PCL fibers in O_2, air and N_2 saturated NaPB solutions.

Table 1
Circuit element values obtained from fitting the EIS spectra in Fig. 2.

$[O_2]$/mM	W/Ω	τ/s	α_w	R/Ω cm^2	CPE/μF cm^{-2} $s^{\alpha-1}$	α
1.3	545	0.8	0.39	1131	50.5	0.92
0.3	575	1.2	0.42	1521	74.3	0.96
0.0	956	1.5	0.44	2015	79.4	1.00

and 0.7 V corresponding to Au oxidation, one reduction peak at 0.1 V corresponding to Au and another reduction peak at −0.65 V attributed to the reduction of dissolved O_2 to OH^- species. The peak intensity value corresponding to the O_2 reduction is higher by a factor of 2 for the Au/PCL compared to the Au bulk electrode.

The scan rate study (Fig. 1B) revealed a linear dependence of the peak current with the square root of the scan rate (10–100 mV s^{-1}), following the equation j_{pc} (mA cm^{-2}) = 0.09 + 6.27 × $v^{0.5}$ (V s^{-1}), R^2 = 0.996, specific for a diffusion controlled process of O_2 reduction. Considering the Randles-Sevčik equation, the diffusion coefficient (D_{O2}) value at 25 °C calculated was 4.6 × 10^{-5} cm^2 s^{-1}.

The electrochemical behavior of Au/PCL in cellular media was also evaluated (results not shown). A different CV profile of Au was observed with a broader oxidation peak at 0.7 V and two reduction peaks, at 0.2 V of Au and one at −0.5 V of O_2, both shifted towards more positive values compared to that in NaPB. This is due to the complexity of the cellular media. However, the reduction process of dissolved O_2 is similar to that observed in 0.1 M NaPB pH 7.0, being controlled by diffusion, with a linear dependency of the peak current with the square root of the scan rate (10–100 mV s^{-1}), following the equation j_{pc} (mA cm^{-2}) = 0.16 + 4.44 × $v^{0.5}$ (V s^{-1}), R^2 = 0.990, with D_{O2} = 2.9 10^{-5} cm^2 s^{-1}, lower than in NaPB. Both D_{O2} values were slightly higher compared with those reported in pure water [17].

Fig. 2C displays CVs recorded at Au/PCL in O_2, air and N_2 saturated solutions, and showed a decrease of the peak with the decrease in dissolved O_2 concentration. Considering the concentrations of dissolved O_2 in solution to be 1.3 mM, 0.25 mM and 0.0 mM in O_2, air and N_2 saturated solutions, respectively, Au/PCL electrode exhibited a linear response to O_2 concentration with current values following the equation j_{pc} (mA cm^{-2}) = 0.17 + 1.37 × $[O_2]$ (mM), R^2 = 0.9996.

3.2.2. Electrochemical impedance spectroscopy

The EIS technique can give valuable information regarding the electrode processes occurring at the electrode/liquid interface [18–20] and can be used as analytical method [21]. EIS spectra were first recorded at Au/PCL in O_2 (1.3 mM), air (0.25 mM) and N_2 (0.0 mM) saturated NaPB, and are shown as complex plane plots in Fig. 2D. The spectra presented diffusional lines in the high to middle frequency range, up to 200 Hz, ending with a semicircle for the medium and low frequency region, which corresponds to the diffusional process and charge transfer process of O_2 at the Au/PCL. Spectra were fitted using an equivalent circuit presented as insert of Fig. 2D, and consisted in R_s in series with a Warburg impedance W, and a RCPE combination. CPE is a constant phase element, defined in [22], corresponding to the pseudo-

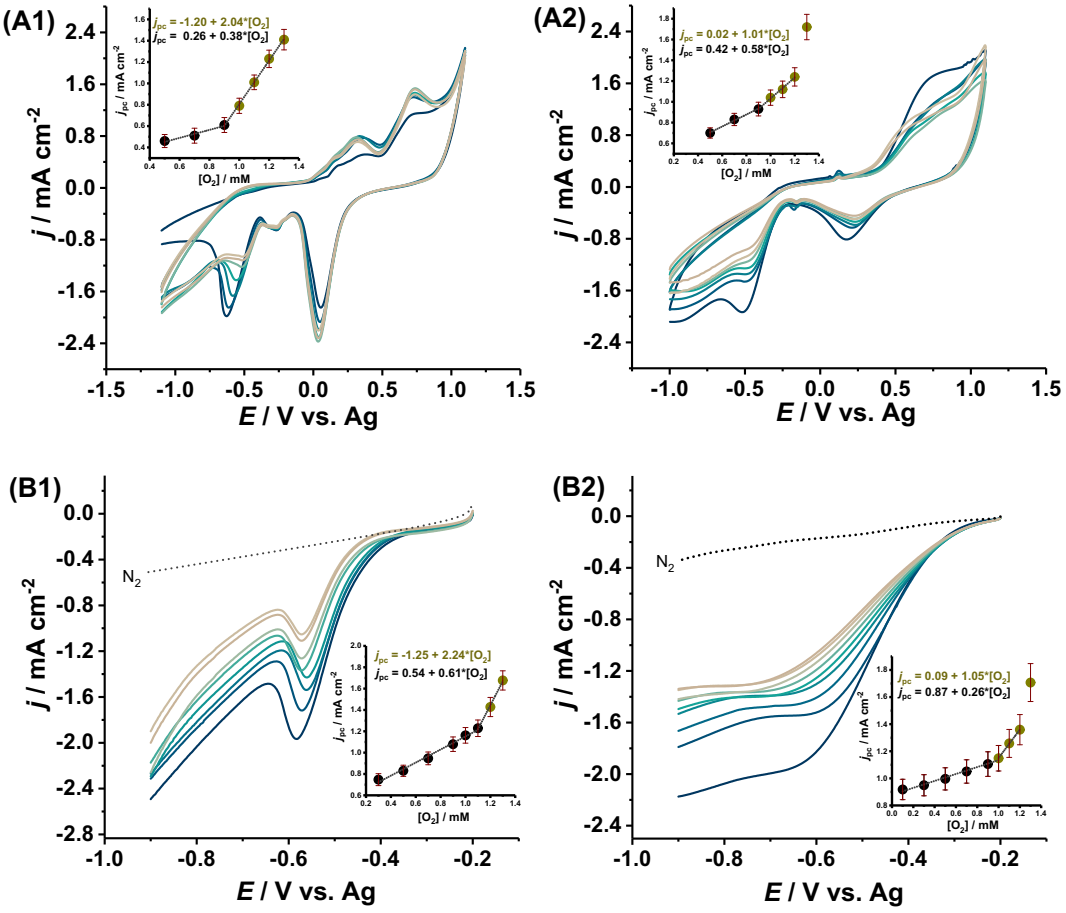

Fig. 3. A) Cyclic and B) Linear sweep voltammograms recorded at Au/PCL in A1,B1 – NaPB and A2,B2 – cellular media upon successive additions of Na_2SO_3 in O_2 saturated solutions (ν = 100 mV s^{-1}).

Table 2
Analytical parameters corresponding to the linear regressions in Fig. 3.

Media	Method	Concentration range/mM	Intercept/mA cm^{-2}	SE	Slope/mA cm^{-2} mM^{-1}	SE	RSD/% (n = 3)
NaPB	CV	0.9–1.3	−1.20	0.05	2.04	0.05	7.2
		0.5–0.9	0.26	0.05	0.38	0.07	7.1
	LSV	1.1–1.3	−1.25	0.17	2.24	0.14	7.6
		0.3–1.1	0.54	0.03	0.61	0.04	7.4
Cellular media	CV	0.9–1.2	0.02	0.05	1.01	0.05	6.3
		0.5–0.9	0.42	0.03	0.58	0.04	6.1
	LSV	0.9–1.2	0.09	0.02	1.05	0.02	8.2
		0.1–0.9	0.87	0.01	0.26	0.02	8.0

capacitance of the Au/PCL in contact with solution and the Warburg impedance *W*, defined as previously described [22], which can be associated to a finite diffusional processes inside the pores of the Au/PCL, depending especially on the fiber network porosity.

The results obtained after fitting the experimental data are shown in Table 1. The values of both *W* and *R* increased upon O_2 removal form the solution, as they are correlated with the diffusional process and charge transfer process of O_2 at the Au/PCL, respectively. A similar effect of dissolved O_2 on the EIS spectra over the mid and high frequency range was reported for a chemisensor [23] based on the conductive polymer poly(azo-Bismark Brown Y) [24].

3.3. Quantification of O_2 at Au/PCL electrodes

3.3.1. Cyclic and linear sweep voltammetry

CVs (Fig. 3A) and LSV (Fig. 3B) were recorded in O_2 saturated NaPB (Fig. 3A1, B1) and in cellular media (Fig. 3A2, B2) upon successive additions of Na_2SO_3 and the parameters for the linear regressions are given in Table 2.

CVs at Au/PCL upon successive additions of Na_2SO_3 into an O_2 saturated NaPB showed a gradual decrease of the cathodic peak corresponding to the O_2 reduction, upon consumption of O_2 by Na_2SO_3 (Fig. 3A1). However, Na_2SO_3 was unable to consume the dissolved O_2 completely on Au/PCL, seen in the O_2 reduction peak stagnation, below 0.5 mM. On bulk Au electrodes, O_2 reduction peak disappears completely for concentrations above 2.6 mM Na_2SO_3. This may be due to the PCL matrix porosity which can lead to O_2 entrapment within the pores. This feature is valuable for PCL application in tissue engineering, especially for tissue implants.

The oxidation and reduction peaks correspondent to Au were not influenced significantly by the Na_2SO_3, a slight increase in their intensity values being observed after first addition, probably due to oxide Au species being reduced by sulfite. The sensor had two linear domains, 1.3–0.9 and 0.9–0.5 mM, with sensitivity values of 2.04 and

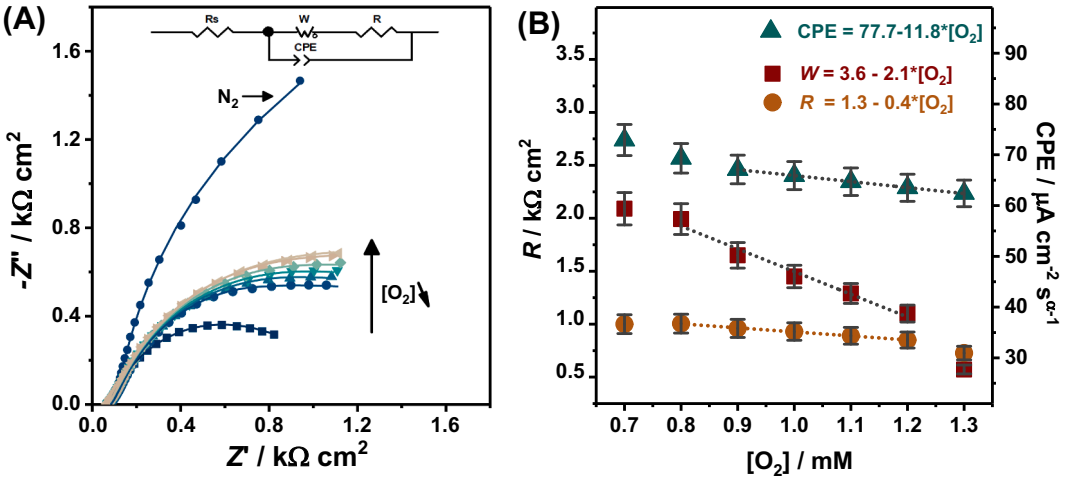

Fig. 4. A) Complex plane impedance plots recorded at −0.4 V with Au/PCL fibers upon successive additions of Na_2SO_3 in O_2 NaPB saturated solution; inset shows the equivalent circuit used to fit the spectra. B) Linear correlation between *R*, *W* and CPE values with O_2 concentration.

Table 3
Circuit element values obtained from fitting the EIS spectra in Fig. 4.

$[O_2]$/mM	W/Ω	τ/s	α_w	R/Ω cm^2	CPE/μF cm^{-2} s$^{\alpha-1}$	α_2
1.3	572	0.9	0.43	945	62.4	0.85
1.2	853	1.7	0.42	1056	63.5	0.85
1.1	1650	1.5	0.48	1157	64.7	0.89
1.0	1650	1.5	0.48	1209	65.9	0.89
0.9	1650	1.6	0.48	1248	67.1	0.89
0.8	1992	1.5	0.5	1307	69.3	0.89
0.7	2090	1.5	0.5	1300	72.9	0.89

0.38 mA cm^{-2} mM^{-1}, respectively (inset Fig. 3A1).

Similar CV measurements were performed in cellular medium (Fig. 3A2), the sensor presenting two linear domains also in this case. The sensitivity value of the linear range 1.1–0.9 mM was lower, of 1.02 mA cm^{-2} mM^{-1}, while the one for the second linear domain, 0.58 mA cm^{-2} mM^{-1}, higher than that obtained in NaPB. The first addition of sulfite in cellular media had a more pronounced effect on sensor response, with a sharper decrease of the peak current corresponding to O_2 reduction. The effect of sulfite on the Au redox peaks was in this case the opposite to that observed in NaPB, a decrease in peak intensity occurring after first sulfite addition probably due to adsorption of species from cellular media on the surface of Au/PCL.

The sensor response in LSV had two linear domains as well (Fig. 3B1), going down to 0.3 mM O_2. Sensitivity values were slightly higher to that obtained by using CV, and were 2.24 and 0.61 mA cm^{-2} mM^{-1}, respectively. In cellular media (Fig. 3B2) sensor sensitivity values were 1.05 and 0.26 mA cm^{-2} mM^{-}1, lower by a factor of two than that obtained in NaPB.

RSD values, corresponding to sensor sensitivity, calculated for 3 different sensors were ≈7%, indicating a good reproducibility of the sensor fabrication. RSD for three different measurements at the same sensor in the same day was lower than 4%, with a good repeatability of the present analytical method.

Results obtained using the Au/PCL for O_2 quantification in cellular media are promising for the applicability of the Au/PCl for O_2 monitoring in cell cultures.

3.3.2. *Electrochemical impedance spectroscopy*

O_2 levels in solution can be also monitored by employing the EIS technique, as already shown in Section 3.2.2 (Fig. 2D). EIS spectra were recorded upon successive additions of Na_2SO_3 in O_2 saturated solution of cellular media and are shown as complex plane impedance plots in Fig. 4A. Spectra were similar to those recorded in NaPB, the same equivalent circuit being used to fit the spectra (see inset of Figs. 4A and 2D) with results shown in Table 3. Sulfite additions lead to changes in the impedance profile only in the middle and low frequency range. As in the case of CV measurements, the first addition of sulfite had more impact on the sensor response, leading to a more pronounced shift in the semicircle magnitude. Following injections had a lower and linear effect on sensor EIS response, with both diffusional resistance (*W*) and charge transfer resistance (*R*) values displaying a linear dependency with the amount of O_2, following the equations: 3.6–2.1 × $[O_2]$, RSD = 7.3%, n = 3 and 1.3–0.4 × $[O_2]$, RSD = 8.9%, n = 3, respectively (Fig. 4B). The values of CPE also decreased linearly by lowering the O_2 concentration (CPE = 77.7–11.8 × $[O_2]$, RSD = 4.2%, n = 3). As in the case of CV study in Section 3.3.1, not all the O_2 could be consumed by Na_2SO_3 additions, explained by PCL matrix porosity, and O_2 entrapment within the pores.

4. Conclusions

Polycaprolacotone electrospun fibers covered with Au by magnetron sputtering exhibited higher electroactive area compared to Au bulk electrodes. O_2 reduction occurred at a negative potential of ≈ −0.7 V vs Ag and is a process controlled by diffusion. By using cyclic and linear sweep voltammetry, the Au/PCL sensor exhibited two linear domains, with higher sensitivities for O_2 levels above 0.9 mM. Electrochemical impedance spectroscopy can also be successfully employed for O_2 quantification using Au/PCL sensors, with diffusional resistance, charge transfer resistance and constant phase element values showing a linear correlation with the amount of dissolved O_2. The electrochemical measurements, both CV and EIS, revealed the possibility to use the PCL matrix as O_2 reservoir for applications such as tissue implants. Moreover, sensor response in cellular media is promising for the applicability of Au/PCL for O_2 monitoring in cellular culture.

CRediT authorship contribution statement

Ariana Serban: Validation, Methodology, Formal analysis, Investigation. **Alexandru Evanghelidis:** Methodology, Investigation. **Melania Onea:** Investigation. **Victor Diculescu:** Resources, Funding acquisition, Writing - review & editing. **Ionut Enculescu:** Resources, Funding acquisition. **Madalina M. Barsan:** Conceptualization, Methodology, Formal analysis, Investigation, Writing - original draft, Supervision, Project administration, Funding acquisition.

Declaration of Competing Interest

The authors declare that they have no known competing financial interests or personal relationships that could have appeared to influence the work reported in this paper.

Acknowledgements

Financial support from the Executive Agency for Higher Education, Research, Development and Innovation Funding (UEFISCDI), Romania, Project code: PN-III-P4-ID-PCE-2016-0580, PN-III-P1-1.2-PCCDI-2017-0697, the Romanian Ministry of Research and Innovation through Operational Programme Competitiveness 2014-2020, Project: NANOBIOSURF-SMIS 103528, and PN19-03 (contract no. 21N/08.02.2019).

References

[1] E. Sapountzi, M. Braiek, J.F. Chateaux, N. Jaffrezic-Renault, F. Lagarde, Recent advances in electrospun nanofiber interfaces for biosensing devices, Sensors (Switzerland) 17 (2017) 1887, https://doi.org/10.3390/s17081887.
[2] A. Evanghelidis, M. Beregoi, V.C. Diculescu, A. Galatanu, P. Ganea, I. Enculescu, Flexible delivery patch systems based on thermoresponsive hydrogels and submicronic fiber heaters, Sci. Rep. 8 (2018) 17555, https://doi.org/10.1038/s41598-018-35914-2.
[3] V.C. Diculescu, M. Beregoi, A. Evanghelidis, R.F. Negrea, N.G. Apostol, I. Enculescu, palladium/palladium oxide coated electrospun fibers for wearable sweat pH-sensors, Sci. Rep. 9 (2019) 8902, https://doi.org/10.1038/s41598-019-45399-2.
[4] M. Beregoi, A. Evanghelidis, V.C. Diculescu, H. Iovu, I. Enculescu, Polypyrrole actuator based on electrospun microribbons, ACS Appl. Mater. Interfaces. 9 (2017) 38068–38075, https://doi.org/10.1021/acsami.7b13196.
[5] M. Beregoi, A. Evanghelidis, E. Matei, I. Enculescu, Polyaniline based microtubes as building-blocks for artificial muscle applications, Sensors Actuators, B Chem. 253 (2017) 576–583, https://doi.org/10.1016/j.snb.2017.06.128.
[6] S. Agarwal, J.H. Wendorff, A. Greiner, Use of electrospinning technique for biomedical applications, Polymer (Guildf.) 49 (2008) 5603–5621, https://doi.org/10.1016/j.polymer.2008.09.014.
[7] R. Murugan, S. Ramakrishna, Nano-featured scaffolds for tissue engineering: a review of spinning methodologies, Tissue Eng. 12 (2006) 435–447, https://doi.org/10.1089/ten.2006.12.435.
[8] Q.P. Pham, U. Sharma, A.G. Mikos, Electrospinning of polymeric nanofibers for tissue engineering applications: a review, Tissue Eng. 12 (2006) 1197–1211, https://doi.org/10.1089/ten.2006.12.1197.
[9] C. Del Gaudio, A. Bianco, M. Folin, S. Baiguera, M. Grigioni, Structural characterization and cell response evaluation of electrospun PCL membranes: micrometric versus submicrometric fibers, J. Biomed. Mater. Res. – Part A 89 (2009) 1028–1039, https://doi.org/10.1002/jbm.a.32048.
[10] M.J. Mochane, T.S. Motsoeneng, E.R. Sadiku, T.C. Mokhena, J.S. Sefadi, Morphology and properties of electrospun PCL and its composites for medical applications: a mini review, Appl. Sci. 9 (2019) 1–17, https://doi.org/10.3390/app9112205.
[11] J.L. Lowery, N. Datta, G.C. Rutledge, Effect of fiber diameter, pore size and seeding method on growth of human dermal fibroblasts in electrospun poly(ε-caprolactone) fibrous mats, Biomaterials 31 (2010) 491–504, https://doi.org/10.1016/j.biomaterials.2009.09.072.
[12] A.R. D'Amato, N.J. Schaub, J.M. Cardenas, E. Franz, D. Rende, A.M. Ziemba, R.J. Gilbert, Evaluation of procedures to quantify solvent retention in electrospun fibers and facilitate solvent removal, Fibers Polym. 18 (2017) 483–492, https://doi.org/10.1007/s12221-017-1061-5.
[13] A.R. D'Amato, M.T.K. Bramson, D.T. Corr, D.L. Puhl, R.J. Gilbert, J. Johnson, Solvent retention in electrospun fibers affects scaffold mechanical properties, Electrospinning 2 (2018) 15–28, https://doi.org/10.1515/esp-2018-0002.
[14] B. Weyand, M. Nöhre, E. Schmälzlin, M. Stolz, M. Israelowitz, C. Gille, H.P. von Schroeder, K. Reimers, P.M. Vogt, Noninvasive oxygen monitoring in three-dimensional tissue cultures under static and dynamic culture conditions, Biores. Open Access. 4 (2015) 266–277, https://doi.org/10.1089/biores.2015.0004.
[15] J. Malda, T.J. Klein, Z. Upton, The roles of hypoxia in the in vitro engineering of tissues, Tissue Eng. 13 (2007) 2153–2162, https://doi.org/10.1089/ten.2006.0417.
[16] C. Busuioc, A. Evanghelidis, A. Galatanu, I. Enculescu, Direct and contactless electrical control of temperature of paper and textile foldable substrates using electrospun metallic-web transparent electrodes, Sci. Rep. 6 (2016) 34584, https://doi.org/10.1038/srep34584.
[17] W. Xing, M. Yin, Q. Lv, Y. Hu, C. Liu, J. Zhang, Oxygen solubility, diffusion coefficient, and solution viscosity, in: W. Xing, G. Yin, J. Zhang (Eds.), Rotating Electrode Methods and Oxygen Reduction Electrocatalysts, Elsevier B.V., 2014, pp. 1–31. doi :10.1016/B978-0-444-63278-4.00001-X0.
[18] M.M. Barsan, E. Matei, M. Enculescu, R. Costescu, N. Preda, T.A. Enache, I. Enculescu, V.C. Diculescu, Nanostructured palladium doped nickel electrodes for immobilization of oxidases through nickel nanoparticles, Electrochim. Acta 315 (2019) 102–113, https://doi.org/10.1016/j.electacta.2019.04.143.
[19] M.M. Barsan, T.A. Enache, N. Preda, G. Stan, N.G. Apostol, E. Matei, A. Kuncser, V.C. Diculescu, Direct immobilization of biomolecules through magnetic forces on Ni electrodes via Ni nanoparticles: applications in electrochemical biosensors, ACS Appl. Mater. Interfaces. 11 (2019) 19867–19877, https://doi.org/10.1021/acsami.9b04990.
[20] M.M. Barsan, V.C. Diculescu, New electrochemical sensor based on CoQ_{10} and cyclodextrin complexes for the detection of oxidative stress initiators, Electrochim. Acta 302 (2019) 441–448, https://doi.org/10.1016/J.ELECTACTA.2019.02.060.
[21] D. Chan, M.M. Barsan, Y. Korpan, C.M.A. Brett, L-lactate selective impedimetric bienzymatic biosensor based on lactate dehydrogenase and pyruvate oxidase, Electrochim. Acta 231 (2017) 205–231, https://doi.org/10.1016/j.electacta.2017.02.050.
[22] M.M. Barsan, R.C. Carvalho, Y. Zhong, X. Sun, C.M.A. Brett, Carbon nanotube modified carbon cloth electrodes: characterisation and application as biosensors, Electrochim. Acta 85 (2012) 203–209, https://doi.org/10.1016/j.electacta.2012.08.048.
[23] A. Olean-Oliveira, M.F.S. Teixeira, Development of a nanocomposite chemiresistor sensor based on Π-conjugated azo polymer and graphene blend for detection of dissolved oxygen, Sensors Actuators, B Chem. 271 (2018) 353–357, https://doi.org/10.1016/j.snb.2018.05.128.
[24] M.F.S. Teixeira, M.M. Barsan, C.M.A. Brett, Molecular engineering of a π-conjugated polymer film of the azo dye Bismarck Brown Y, RSC Adv. 6 (2016) 101318–101322, https://doi.org/10.1039/c6ra20335c.